Effect of Adsorption Mechanism on Conduction in Single-Molecule Pyrrole-Based Sensor for AFB1

Effect of Adsorption Mechanism on Conduction in Single-Molecule Pyrrole-Based Sensor for AFB1

Fabrizio Mo, *Graduate Student Member, IEEE*, Yuri Ardesi, *Member, IEEE*, Chiara Elfi Spano, Massimo Ruo Roch, *Member, IEEE*, Gianluca Piccinini, and Mariagrazia Graziano

***Abstract*—We investigate through *ab-initio* simulations the gold-8PyrroleDiThiol-gold (Au-8PyDT) molecular quantum dot as an amperometric single-molecule sensor for the aflatoxin B1 (AFB1) detection. We study the chemical-physical interaction of AFB1 with the Au-8PyDT, and we analyze the transport characteristics of the four most probable adsorption configurations. We also investigate the link between transport modulation and adsorption mechanism. Interestingly, the investigated sensor exhibits conduction features similar to other types of quantum dot-based sensors. A significant current suppression occurs in all cases, with almost two orders of magnitude of current decrease in presence of AFB1 at 0.6 V. Considering the sensor robustness w.r.t. the specific adsorption configurations, our study motivates future research in this field.**

***Index Terms*—Adsorption, AFB1, aflatoxin, amperometric sensor, electronic transport, molecular electronics, pyrrole, quantum transport, sensor, single-molecule.**

I. Introduction

AFLATOXINS are carcinogenic secondary metabolites of *Aspergillus flavus* and *Aspergillus parasiticus* fungi. Among them, aflatoxin B1 (AFB1) is the most hazardous one, and it is most frequently found in contaminated food [1], [2].

Standard AFB1 detection methods require skilled technicians who perform appropriate extraction and clean-up methods, with measurement through high-cost and bulky instrumentation. Current research efforts are toward high sensitivity and fast AFB1 detection, possibly permitting an automatization in the measurement process [3], [4]. Novel bio-sensors, also exploiting nanomaterials, were developed. Nevertheless, drawbacks are still present: high fabrication cost, toxicity of the employed nano-elements, and complex sensor functionalization techniques [5], [6]. In electrical detection of AFB1, it was experimentally proven that the sensitivity can be improved when detection element size is scaled down, e.g., from large bio-molecules as antibodies to small nano-body molecules [6].

At the same time, advancements in supra- and single-molecule electronics are filling the gap between theoretical investigations and prototyping, pushing researchers to study electrical single-molecule detection [7]. It would achieve the ultimate limit of chemical sensitivity, i.e., the detection of single molecules, by monitoring an electrical current [8], [9], [10], [11], [12].

In this scenario, in our preliminary work [13], we found the gold-8-Pyrrole-DiThiol-gold molecular dot (Au-8PyDT) promising as an amperometric Single-Molecule Sensor (SMS) for AFB1 detection. We chose pyrrole as detection element because of its synthesis simplicity, already-proven sensing capability and non-toxicity [14], [15], [16]. We selected gold as electrode material since it is proven to be effective in molecular electronics at the experimental level and it is an inert metal, suitable for sensing [17], [18], [19], [20]. We obtained high AFB1 sensitivity in terms of current modulation at the level of a single AFB1 molecule. In addition, in [21], we have theoretically proven an impressive increase of the Au-8PyDT sensitivity through a strongly coupled gate terminal.

In the present work, in sight of prototype fabrication, we address again the two-terminal Au-8PyDT. Indeed, it is challenging to obtain high-quality and very thin gate dielectrics to ensure strong, reliable and reproducible gate coupling to reach the performance motivating the high costs of gate structure fabrication. Whereas, the two-terminal Au-8PyDT matches feasible experimental structures, that we are resolved to address in future works. In particular, we clarify for the first time the nature of the chemical-physical AFB1-SMS interaction and its influence on electronic transport. In addition, we address the sensor reliability toward chemical noise, by comparing the results obtained for the most probable adsorption configurations. Our outcomes provide useful insights into the functioning of the proposed SMS, toward sensor engineering and prototyping. Selectivity should be investigated in the future through the developed methodology, verifying an exclusive current modulation to AFB1 with sufficient noise margins.

II. Methodology and Computational Details

Fig. 1(a)–(c) report the considered Au-8PyDT SMS geometry. The gold nanogap size, 33.5 Å, is chosen according to experimental values [22], [23] and matches the 8PyDT length. We suppose to chemically bond a chain of 8 pyrrole monomers (8Py) to source (S) and drain (D) gold electrodes through thiol

Manuscript received 8 September 2023; accepted 21 November 2023. Date of publication 24 November 2023; date of current version 5 December 2023. The review of this article was arranged by Associate Editor X. Liu. *(Fabrizio Mo, Yuri Ardesi, and Chiara Elfi Spano contributed equally to this work.) (Corresponding author: Fabrizio Mo.)*

Fabrizio Mo, Yuri Ardesi, Chiara Elfi Spano, Massimo Ruo Roch, and Gianluca Piccinini are with the Department of Electronics and Telecommunications, Politecnico di Torino, 10129 Turin, Italy (e-mail: fabrizio.mo@polito.it; yuri.ardesi@polito.it; chiaraelfi.spano@polito.it; massimo.ruoroch@polito.it; gianluca.piccinini@polito.it).

Mariagrazia Graziano is with the Department of Applied Science and Technology, Politecnico di Torino, 10129 Turin, Italy (e-mail: mariagrazia.graziano@polito.it).

This article has supplementary downloadable material available at https://doi.org/10.1109/TNANO.2023.3336522, provided by the authors.

Digital Object Identifier 10.1109/TNANO.2023.3336522

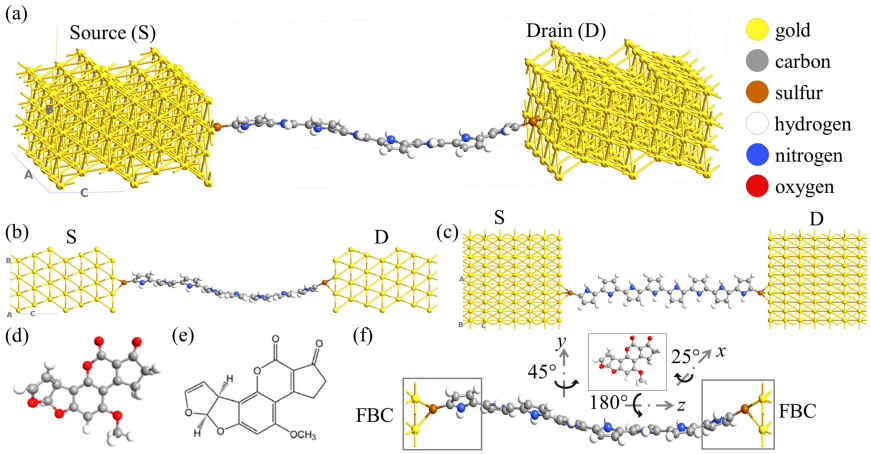

Fig. 1. (a) Au-8PyDT geometry; (b) Au-8PyDT side view; (c) Au-8PyDT top view; (d) AFB1; (e) AFB1 structural formula; (f) Adsorption study strategy.

anchoring groups (8-pyrrole-dithiol, 8PyDT), as experimentally proven in [24] for a pyrrole self-assembled monolayer. The device is thus a single-molecule junction (Au-8PyDT) used as a molecular quantum dot sensor. Fig. 1(d) and (e) show the AFB1 molecule and its structural formula. We investigate the SMS-AFB1 interaction in terms of AFB1 adsorption onto the 8PyDT - see Fig. 1(f). Compared to our previous works [13], [21], in this work, we consider additional adsorption configurations, which cover all possible AFB1-8PyDT relative orientations. In particular, y rotations with 45° step, and z rotations with 180° step are considered. The latter operation corresponds to flipping the AFB1 molecule over the 8PyDT. We do not consider intermediate rotation steps in z, since we have already verified that the 8PyDT and AFB1 interaction is more stable when AFB1 is in a π-stack fashion configuration [21] (maximum steric overlap). Moreover, we do not consider additional x rotations, since, considering the 8PyDT bending, it would result in unrealistic atom overlapping between AFB1 and 8PyDT with Pauli and nuclei repulsion.

All the calculations are performed in QuantumATK [25]. The adsorption geometries are relaxed using Density-Functional-Theory (DFT) within the Generalized Gradient Approximation (GGA), with Perdew–Burke–Ernzerhof (PBE) functional, and polarized double-ζ (DZP) basis set for all elements except for gold, for which polarized single-ζ (SZP) basis set is used. We model the entire gold electrodes by enforcing Fixed Boundary Conditions (FBC) for the atoms in the two lateral regions of the Au-8PyDT - Fig. 1(f). All other atoms are free to relax with no constraints, exploiting the LBFGS algorithm with a force tolerance of $0.05\,\mathrm{eV/Å}$. The van der Waals Grimme D3 and the counterpoise (CP) correction for Basis Set Superposition Error (BSSE) are used. We calculate the adsorption energy E_{ads} as:

$$E_{ads} = E_{AFB1/SMS} - [E_{AFB1} + E_{SMS}] \qquad (1)$$

where $E_{AFB1/SMS}$ is the total energy for the AFB1 adsorbed onto the Au-8PyDT SMS, E_{AFB1} and E_{SMS} are the total energy of the isolated AFB1 and Au-8PyDT SMS, respectively.

Chemical competitors and noise may affect the adsorption process and the final AFB1 adsorption configuration, which may differ from being the most stable and probable one. To account for the effects of chemical-physical competitors we consider the four most stable adsorption configurations, which we call AC1 (most stable), AC2 (second most stable), AC3 (third most stable) and AC4 (fourth most stable). Therefore, we analyze and compare the sensor response in all the cases.

The electronic transport study is performed through the purely quantum and general Non-Equilibrium Green's Function (NEGF) formalism. Within the DFT+NEGF framework, we self-consistently solve the electronic structure, the transport and the electrostatic equations until convergence over the system Hamiltonian is reached with an energy tolerance of 10^{-4}. We use DFT, GGA, PBE with D3, SZP for Au and DZP for other elements, recursion self-energy calculator, Monkhorst k-grid with [4, 4, 150] density in equilibrium, transverse [12, 12] density in non-equilibrium increased to [17, 17] on non-convergence. The system electrostatics is modeled through the Poisson equation (conjugate gradient solver), with periodic boundary conditions in the transverse horizontal direction, to model the electrode's physical extension. Dirichlet boundary conditions are used in the transport direction and along the transverse vertical direction to avoid simulation artifacts due to the presence of AFB1 molecule. We calculate the electrical current I_{DS} with the Landauer-like formula [26]:

$$I_{DS} = \frac{2q}{h} \int_{-\infty}^{+\infty} T(E, V_{DS}) \left[f_S(E) - f_D(E) \right] dE \qquad (2)$$

where q is the electron charge, h is the Planck constant, E is the electron energy, V_{DS} the applied voltage, f_S and f_D are source and drain Fermi-Dirac distributions, respectively. $T(E, V_{DS})$ is the transmission spectrum (TS), representing the S-to-D electron transmission probability. It depends on the electron energy E and the applied voltage V_{DS}. The current variation $\Delta I_{DS} = I_{DS,AFB1} - I_{DS,0}$ and the ratio $I_{DS,AFB1}/I_{DS,0}$ are used to characterize the sensor response. $I_{DS,0}$ is the Au-8PyDT current, and $I_{DS,AFB1}$ is the current in presence of AFB1. The sensor

recovery time τ is estimated as (details in section SI 1):

$$\tau \approx \nu^{-1}\, exp\left(\frac{|E_{ads}|}{kt}\right) \quad (3)$$

where ν is the AFB1 desorption attempt frequency (assumed in the range $10^{12} \div 10^{14}$ Hz), k is the Boltzmann's constant and t the temperature. To investigate the AFB1-SMS interaction, the mechanism of current modulation and the link between them, we use well-established analysis tools in molecular- and nano-electronics (details in section SI 1): Mulliken Population (MP), Electron Density (ED), Electron Density Difference (EDD), Electron Localization Function (ELF), Transmission Eigenstates (TEs) and Transmission Pathways (TPs).

III. Working Principle and Sensor Response

A positive V_{DS} lowers the D Fermi level (E_{FD}) w.r.t. the S one (E_{FS}) of an amount $-qV_{DS}$ ($E_{FD} = E_{FS} - qV_{DS}$), that we call Bias Window (BW): BW$= qV_{DS}$. The V_{DS} affects (2) through the Fermi function difference:

$$f_S(E) - f_D(E) = \frac{1}{e^{\frac{E-E_{FS}}{kt}}+1} - \frac{1}{e^{\frac{E-E_{FS}+qV_{DS}}{kt}}+1} \quad (4)$$

An I_{DS} originates if f_S and f_D are unbalanced, with occupied states at S and empty states at D, and if the TS is large enough to ensure a significant S-to-D transmission probability. In particular, the S-to-D electronic transport occurs through 8PyDT states, at a given E, for which transmission resonances occur (with TS peaks). The effect of the Fermi function difference in (2) is to weight $T(E, V_{DS})$. For energies E inside or close to the BW, the Fermi function difference is close to unity ($f_S(E) - f_D(E) \approx 1$), while for energies E distant from the BW it is close to zero ($f_S(E) - f_D(E) \approx 0$). Therefore, transmission occurs for E values in the BW that correspond to 8PyDT states, with large TS. The sensing mechanism relies on TS modifications at energies E inside the BW produced by the AFB1 presence. From (2), such modifications correspond to a different current I_{DS}, making possible the amperometric detection of AFB1. Additional details and a detailed explanation of why the sensor response is voltage-dependent are provided in [13] and summarized in section SI 1. In the present work, we clarify how the AFB1-SMS interaction affects $T(E, V_{DS})$ and I_{DS} and we investigate the robustness of such a mechanism by considering the four most probable sensing configurations.

IV. Results and Discussion

Table I reports the calculated adsorption energies E_{ads}, as defined in (1). For completeness, we report the E_{ads} calculated in our previous works [13], [21] in Table SI2. Comparing the results of Table I and Table SI2, we identify the four most stable adsorption configurations: AC1 with X $= 0°$, Y $= 45°$, Z $= 180°$ and $E_{ads} = -119.89$ kJ/mol; AC2 with X $= 0°$, Y $= 0°$, Z $= 0°$ and $E_{ads} = -102.94$ kJ/mol; AC3 with X $= 0°$, Y $= 180°$, Z $= 180°$ and $E_{ads} = -101.75$ kJ/mol; AC4 with X $= 0°$, Y $= 315°$, Z $= 0°$ and $E_{ads} = -101.09$ kJ/mol - bold in Table I. In all four cases, E_{ads} is in between strong physisorption and typical chemisorption energy, and it is compatible with hydrogen bond energy [27], [28].

TABLE I
Calculated E_{ads} Values; X is Fixed to $0°$ (X $= 0°$) in This Work

Geometry	E_{ads} (kJ/mol)	Geometry	E_{ads} (kJ/mol)
Z=0°, Y=0°	**-102.94**	Z=180°, Y=0°	-78.58
Z=0°, Y=45°	-95.96	**Z=180°, Y=45°**	**-119.89**
Z=0°, Y=90°	-89.83	Z=180°, Y=90°	-90.85
Z=0°, Y=135°	-95.87	Z=180°, Y=135°	-85.02
Z=0°, Y=180°	-99.64	**Z=180°, Y=180°**	**-101.75**
Z=0°, Y=225°	-85.97	Z=180°, Y=225°	-92.95
Z=0°, Y=270°	-85.79	Z=180°, Y=270°	-88.72
Z=0°, Y=315°	**-101.09**	Z=180°, Y=315°	-77.69

Even if AFB1 is experimentally proven to form hydrogen bonds with organic detection elements [29], [30], and even if the obtained E_{ads} are compatible with hydrogen bond formation, we further investigate the nature of the AFB1-8PyDT interaction. Fig. 2(a) reports the AC1 optimized geometry. If compared with the isolated 8PyDT geometry -Fig. 1(a)- three important differences are present: i) The 4th and 5th pyrrole rings are rotated the one w.r.t. the other of 121.98° - inset of Fig. 2(a). The same angle is 98.78° in the isolated case. ii) The 4th pyrrole ring presents a slightly longer N-H bond length: 1.03 Å versus the 1.01 Å of the isolated case. iii) The AFB1 carbonyl groups present a slightly longer C=O bond length: 1.23 Å versus the 1.22 Å of the isolated case. We relate such modifications to the attractive interaction performed by the slightly negatively charged carbonyl groups of AFB1 on the slightly positively charged secondary amines of the 8PyDT molecule. In this perspective, the AC1 geometry can be explained as an incipient proton transfer reaction, in which the NH of the 4th pyrrole ring acts as the proton donor, and the AFB1 (actually its carbonyl groups) as the acceptor. This is in agreement with Steiner's definition of hydrogen bond only if there is also evidence of a local bond [28]. To investigate the presence of a local bond, we consider additional analyses. The MPs in Fig. 2(b) and (c) show no substantial difference of atomic charge in the 8PyDT when AFB1 is present. Therefore, no significant charge transfer occurs between the 8PyDT and the AFB1. The ED in Fig. 2(d) and the EDD in Fig. 2(e) do not highlight the presence of covalent interaction nor electron sharing between the 8PyDT and the AFB1. The ELFs in Fig. 2(f) and (g) show again no substantial difference of electron delocalization in the 8PyDT when AFB1 is present. Since there is no evidence of an existing bond interaction we conclude that the 8PyDT-AFB1 interaction is of van der Waals type, and considering the order of magnitude of E_{ads} we conclude that the AFB1 is strongly physisorbed onto the 8PyDT detection element.

Similar considerations are true for the other considered adsorption configurations, i.e. AC2, AC3, AC4. We report the results in Fig. SI3, SI4, SI5. Geometrical differences are again related mainly to significant ring rotations and small bond length variations, while MP, ED, EDD, ELF do not show the presence of any bond between the 8PyDT and the AFB1. Therefore, in all cases, the 8PyDT-AFB1 interaction is of van der Waals type. The system energetics in Table SI6 is in agreement with this result. Indeed, the dominant energy component in all cases is electrostatics in nature. Even if this is often true in hydrogen

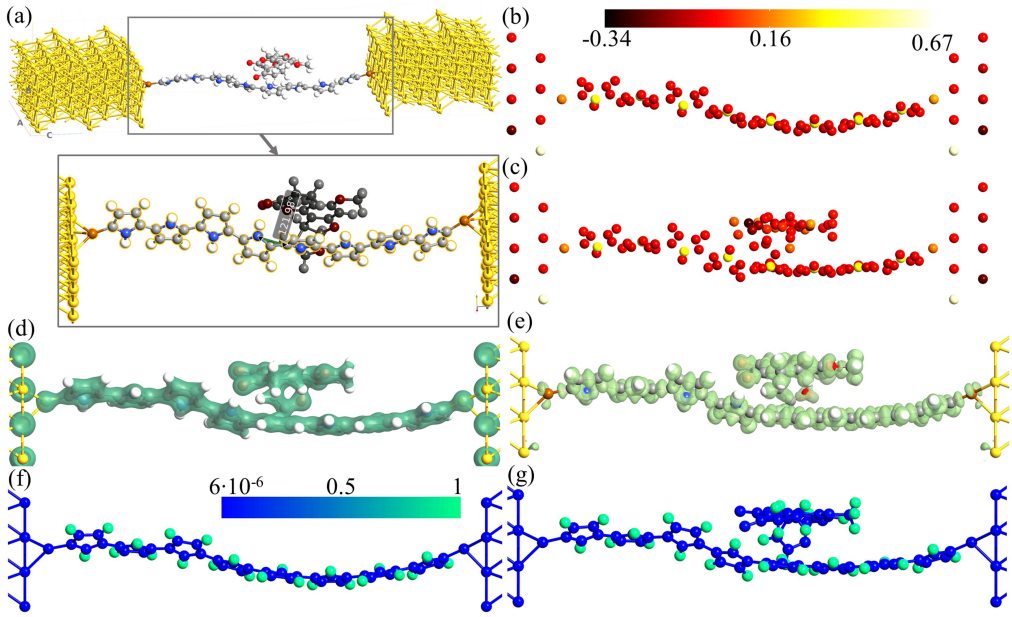

Fig. 2. (a) AC1 geometry - the inset highlight the differences w.r.t. to isolated sensor; Mulliken atomic charge: (b) Au-8PyDT, (c) AC1; (d) AC1 electron density (90%); (e) AC1 electron density difference; ELF: (f) Au-8PyDT, (g) AC1.

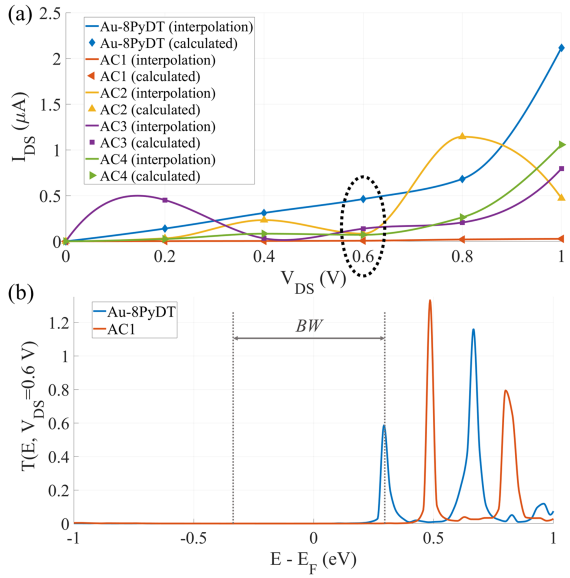

Fig. 3. (a) $I_{DS}(V_{DS})$ curves; (b) $T(E)$ at fixed $V_{DS} = 0.6\,\mathrm{V}$.

bonds, it is also extensively compatible with the van der Waals nature of the interactions.

Fig. 3(a) reports the calculated $I_{DS}(V_{DS})$ characteristics and their Hermite cubic shape-preserving interpolations [31]. At low V_{DS} the AC3 current is greater than the isolated Au-8PyDT one, while the AC2, AC3, AC4 current is lower. At $V_{DS} = 0.4\,\mathrm{V}$ the AC2 current approaches the Au-8PyDT one. Both these situations are undesired since it is difficult to discriminate the case in which there is AFB1 (AC1, AC2, AC3, AC4) from the one in which it is not present (Au-8PyDT). Whereas, at $V_{DS} = 0.6\,\mathrm{V}$ the I_{DS} with AC1, AC2, AC3 and AC4 is significantly

TABLE II
ΔI_{DS} AND $I_{DS,AFB1}/I_{DS,0}$ AT $V_{DS} = 0.6\,\mathrm{V}$

	AC1	AC2	AC3	AC4
ΔI_{DS} (nA)	-455.6	-378.6	-324.1	-391.0
$I_{DS,AFB1}/I_{DS,0}$ (a.u.)	0.014	0.181	0.299	0.154

lower than the Au-8PyDT one and the ΔI_{DS} is maximum in magnitude. Therefore, 0.6 V can serve as the operating voltage for the AFB1 detection for all the adsorption configurations. Table II reports the ΔI_{DS} and the $I_{DS,AFB1}/I_{DS,0}$ ratio at $V_{DS} = 0.6\,\mathrm{V}$ - see Fig. SI7 for additional V_{DS}. In all cases, the current modulation is of the order of hundreds of nA, and it is detectable with conventional electronics [9]. In the AC1 case, the current suppression is the largest: almost two orders of magnitude from $0.462\,\mu\mathrm{A}$ to $6.56\,\mathrm{nA}$, with $I_{DS,AFB1}/I_{DS,0} = 0.014$, meaning that more than 98% of current suppression occurs. The smallest ΔI_{DS} (AC3) corresponds to a two-thirds current reduction from $0.462\,\mu\mathrm{A}$ to $0.138\,\mu\mathrm{A}$ (with $I_{DS,AFB1}/I_{DS,0} = 0.299$).

To understand the origin of such current modulations we investigate the transport properties of the system. Fig. 3(b) reports the TS for the Au-8PyDT and of the AC1 at $V_{DS} = 0.6\,\mathrm{V}$. The AFB1 presence shifts the TS peaks toward higher energies, so they do not fall inside the BW anymore. Even if the lowest energy peak is increased in magnitude in the AC1 case, it is weighted by the Fermi function difference in (2), thus a strong I_{DS} reduction occurs.

We investigate in detail the transport features in Fig. 4. In the Au-8PyDT case, we consider the largest TS peak within the BW, i.e. the one at $E = 0.293\,\mathrm{eV}$ (half included in the BW). This TS peak is composed by several transmission coefficients - see section SI1. We consider the largest one and the corresponding TE, which we report in Fig. 4(a) and (c). We carry

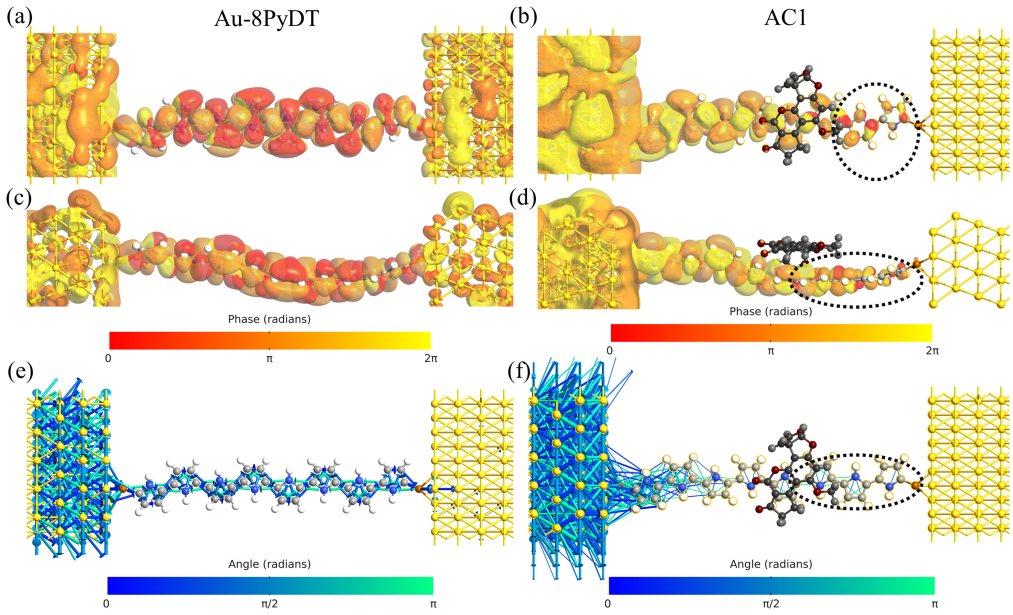

Fig. 4. Au-8PyDT main TE within the considered BW: (a) top view, (c) side view; AC1 main TE within the considered BW: (b) top view, (d) side view; TP for Au-8PyDT (e) and AC1 (f).

out a similar procedure for the AC1 case. Since in Fig. 3(b) there is no appreciable TS peak in the BW, we consider the graph in logarithmic scale - Fig. SI8. We identify the largest transmission coefficient within the BW (arrow in Fig. SI8) and the corresponding TE, which we report in Fig. 4(b) and (d). By comparison of the two TEs we notice that in the Au-8PyDT case, the TE is uniform along the 8PyDT, with almost constant iso-probability surface. Whereas, in the AC1 case, it gradually reduces from left (S) contact to right (D) one. In addition, a phase change in the TE lobes is required to transmit electrons (color change in the circled region). At D side very small transmission occurs. The TP analysis (for the same selected E values) shows that for Au-8PyDT, a uniform transmission occurs from S to D, with dominating S-to-D TPs. Instead, in the AC1 case, the larger the distance from the S, the lower the S-to-D transmission is. A strong decrease occurs around the 3rd and the 4th pyrrole rings. This is where the AFB1 mainly affects the 8PyDT geometry. Thus, we suppose the TS and I_{DS} reduction to be related to the 8-PyDT torsion. Also, the TS energy shift can be related to the 8PyDT torsion. Indeed, torsion in conjugated molecules results in a certain degree of conjugation breaking, and the electrons in the π orbitals gain extra energy and angular momentum because of the orbital increased curvature. Moreover, it is known that the device portion that mainly influences the TS is the one with fewer electron states - the molecular channel [26], [32]. Therefore, an upward shift of the 8-PyDT energy levels should reflect a corresponding shift of the resonant TS peaks. Similar considerations are also true, even if less marked, in the AC2, AC3 and AC4 cases. We report for completeness the TS in linear and logarithmic scale in Fig. SI9 and the detailed transport analyses in Fig. SI10. From our results, there is no specific link between the adsorption mechanism (physisorption) and the transport modulation, which is instead related to a conformation or steric change of the 8PyDT.

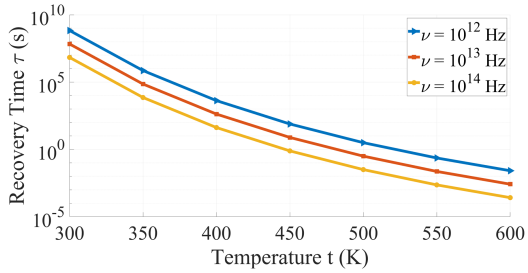

Fig. 5. Sensor recovery time in function of t for $E_{ads} = -119.89\,\mathrm{kJ/mol}$.

Fig. 5 reports τ in function of t, parametrized w.r.t. ν. At the supposed operating t (300 K), the AFB1 sensing is stable, with τ longer than 78 days for all the ν. To enhance the recovery process, the sensor can be heated, as normally done [33], [34]. At 400 K, τ is in between 42 s ($\nu = 10^{14}$ Hz) and 4200 s ($\nu = 10^{12}$ Hz). At 450 K, τ is below 78 s for all the ν. A recovery temperature of around 450 K can be used to regenerate the sensor after the sensing. However, pyrrole thin films present phase transition around 150 ÷ 300 °C (420 ÷ 570 K) depending on the synthesis process and dopants [14]. Thus, future works should verify the effect of temperature on a single polymeric chain and eventually investigate other ways to supply the desorption energy, e.g., electrodesorption [35].

V. Conclusion

We investigated through *ab initio* calculations the Au-8PyDT molecular quantum dot as an amperometric Single-Molecule Sensor (SMS) for the AFB1 detection. To account for competitor stochastic processes, we selected the four most stable adsorption configurations and we studied the chemical-physical interaction and transport properties. Strong physisorption is the main mediating adsorption mechanism, and the AFB1 significantly

affects the I_{DS}. A current reduction of almost two orders of magnitude, from $0.462\,\mu\text{A}$ to $6.56\,\text{nA}$, is present in the optimum sensing condition, corresponding to AC1 configuration at 0.6 V. Interestingly, the transport modulation seems independent on the nature of the AFB1-8PyDT chemical interaction, while we believe it is caused by an 8PyDT torsion, that breaks the 8PyDT conjugation and affects the molecular channel conformation and orbitals, with spatial TEs and TPs modulation. Despite the very different sensor structure, this is coherent with the results we obtained in a previous work [36]. Thanks to the effective I_{DS} reduction of hundreds of nA in all the AC1, AC2, AC3, AC4 cases, the proposed SMS is promising for chemically robust, label-free, pervasive detection of AFB1 concentration in food stocks and on field. The SMS reacts to a single AFB1 molecule. In our vision, to precisely quantify the AFB1 concentration, we believe a matrix of SMSs can be used along with statistics post-processing occurring on an integrated chip Considering the non-toxicity and simple synthesis of pyrrole, and the potential single-molecule sensitivity, we believe the explored SMS is promising for future research, that should focus on selectivity toward other aflatoxins and chemical competitors and on the experimental proof of the theorized sensor.

REFERENCES

[1] W. H. Organization and S. Joint FAO/WHO Expert Committee on Food Additives, *Eval. of Certain Contaminants in Food: Eighty-Third Rep. of the Joint FAO/WHO Expert Committee on Food Additives*. Geneva, Switzerland: World Health Org., 2017.

[2] IARC Working Group on the Evaluation of Carcinogenic Risks to Humans, "Some traditional herbal medicines, some mycotoxins, naphthalene and styrene," *IARC Work. Group on the Eval. of Carcinogenic Risks to Humans*, vol. 82. Geneva, Switzerland: WHO, 2002, pp. 1–556.

[3] Q. Wang, Q. Yang, and W. Wu, "Progress on structured biosensors for monitoring aflatoxin B1 from biofilms: A review," *Front. Microbiol.*, vol. 11, 2020, Art. no. 408.

[4] G. Miklós et al., "Detection of aflatoxins in different matrices and food-chain positions," *Front. Microbiol.*, vol. 11, 2020, Art. no. 1916.

[5] C. Yan, Q. Wang, Q. Yang, and W. Wu, "Recent advances in aflatoxins detection based on nanomaterials," *Nanomaterials*, vol. 10, no. 9, 2020, Art. no. 1626.

[6] Z. Xue et al., "Recent advances in aflatoxin B1 detection based on nanotechnology and nanomaterials-a review," *Analytica Chimica Acta*, vol. 1069, pp. 1–27, 2019.

[7] Y. Li, C. Yang, and X. Guo, "Single-molecule electrical detection: A promising route toward the fundamental limits of chemistry and life science," *Accounts Chem. Res.*, vol. 53, no. 1, pp. 159–169, 2020.

[8] J. J. Gooding and K. Gaus, "Single-molecule sensors: Challenges and opportunities for quantitative analysis," *Angewandte Chemie Int. Ed.*, vol. 55, no. 38, pp. 11354–11366, 2016.

[9] C. W. Fuller et al., "Molecular electronics sensors on a scalable semiconductor chip: A platform for single-molecule measurement of binding kinetics and enzyme activity," *Proc. Nat. Acad. Sci.*, vol. 119, no. 5, 2022, Art. no. e2112812119.

[10] N. Xin et al., "Tuning charge transport in aromatic-ring single-molecule junctions via ionic-liquid gating," *Angewandte Chemie Int. Ed.*, vol. 57, no. 43, pp. 14026–14031, 2018.

[11] F. Mo, C. E. Spano, Y. Ardesi, G. Piccinini, and M. Graziano, "Beyond-CMOS artificial neuron: A simulation- based exploration of the molecular-FET," *IEEE Trans. Nanotechnol.*, vol. 20, pp. 903–911, 2021.

[12] V. Cauda, P. Motto, D. Perrone, G. Piccinini, and D. Demarchi, "pH-triggered conduction of amine-functionalized single ZnO wire integrated on a customized nanogap electronic platform," *Nanoscale Res. Lett.*, vol. 9, no. 1, pp. 1–10, Jan. 2014.

[13] F. Mo et al., "Single-molecule aflatoxin B1 sensing via pyrrole-based molecular quantum dot," in *Proc. IEEE 22nd Int. Conf. Nanotechnol.*, 2022, pp. 153–156.

[14] T. V. Vernitskaya and O. N. Efimov, "Polypyrrole: A conducting polymer; its synthesis, properties and applications," *Russian Chem. Rev.*, vol. 66, no. 5, pp. 443–457, May 1997.

[15] A. Fahlgren et al., "Biocompatibility of polypyrrole with human primary osteoblasts and the effect of dopants," *PLoS One*, vol. 10, no. 7, pp. e0134023–e0134023, 2015.

[16] X. Wang et al., "Evaluation of biocompatibility of polypyrrole in vitro and in vivo," *J. Biomed. Mater. Res. A*, vol. 68, no. 3, pp. 411–422, Mar. 2004.

[17] T. Böhler, J. Grebing, A. Mayer-Gindner, H. v Löhneysen, and E. Scheer, "Mechanically controllable break-junctions for use as electrodes for molecular electronics," *Nanotechnology*, vol. 15, no. 7, pp. S465–S471, May 2004.

[18] I. Rattalino, P. Motto, G. Piccinini, and D. Demarchi, "A new validation method for modeling nanogap fabrication by electromigration, based on the resistance–voltage (R–V) curve analysis," *Phys. Lett. A*, vol. 376, no. 30, pp. 2134–2140, 2012.

[19] D. Demarchi, P. Civera, G. Piccinini, M. Cocuzza, and D. Perrone, "Electrothermal modelling for EIBJ nanogap fabrication," *Electrochimica Acta*, vol. 54, no. 25, pp. 6003–6009, 2009.

[20] B. Hammer and J. K. Norskov, "Why gold is the noblest of all the metals," *Nature*, vol. 376, no. 6537, pp. 238–240, Jul. 1995.

[21] F. Mo et al., "Design of Pyrrole-based gate-controlled molecular junctions optimized for single-molecule aflatoxin B1 detection," *Sensors*, vol. 23, no. 3, 2023, Art. no. 1687.

[22] D. Xiang et al., "Three-terminal single-molecule junctions formed by mechanically controllable break junctions with side gating," *Nano Lett.*, vol. 13, no. 6, pp. 2809–2813, 2013.

[23] V. Dubois et al., "Massively parallel fabrication of crack-defined gold break junctions featuring sub-3 nm gaps for molecular devices," *Nature Commun.*, vol. 9, no. 1, 2018, Art. no. 3433.

[24] B. Vercelli, G. Zotti, A. Berlin, and S. Grimoldi, "Polypyrrole self-assembled monolayers and electrostatically assembled multilayers on gold and platinum electrodes for molecular junctions," *Chem. Mater.*, vol. 18, no. 16, pp. 3754–3763, Aug. 2006.

[25] S. Smidstrup et al., "QuantumATK: An integrated platform of electronic and atomic-scale modelling tools," *J. Phys.: Condens. Matter*, vol. 32, no. 1, Oct. 2019, Art. no. 015901.

[26] S. Datta, *Quantum Transport: Atom to Transistor*. Cambridge, U.K.: Cambridge Univ. Press, 2005, doi: 10.1017/CBO9781139164313.

[27] A. Zangwill, *Physics At Surfaces*. Cambridge, U.K.: Cambridge Univ. Press, 1988.

[28] T. Steiner, "The hydrogen bond in the solid state," *Angewandte Chemie Int. Ed.*, vol. 41, no. 1, pp. 48–76, 2002.

[29] F. Ciriaco et al., "An in-silico pipeline for rapid screening of DNA aptamers against mycotoxins: The case-study of fumonisin B1, aflatoxin B1 and ochratoxin A," *Polymers*, vol. 12, no. 12, 2020, Art. no. 2983.

[30] L. Ma, J. Wang, and Y. Zhang, "Probing the characterization of the interaction of aflatoxins B1 and G1 with calf thymus DNA in vitro," *Toxins*, vol. 9, no. 7, 2017, Art. no. 209.

[31] F. N. Fritsch and R. E. Carlson, "Monotone piecewise cubic interpolation," *SIAM J. Numer. Anal.*, vol. 17, no. 2, pp. 238–246, 1980.

[32] C. E. Spano, Y. Ardesi, G. Piccinini, and M. Graziano, "Enhancing the on/off current ratio in single-molecule FET via destructive quantum interference," *IEEE Trans. Electron Devices*, vol. 69, no. 10, pp. 5906–5912, Oct. 2022.

[33] K. Wetchakun et al., "Semiconducting metal oxides as sensors for environmentally hazardous gases," *Sensors Actuators B: Chem.*, vol. 160, no. 1, pp. 580–591, 2011.

[34] R. Guarino et al., "Modelling electronic transport in monocrystalline metal oxide gas sensors: From the surface kinetics to the experimental response," *Sensors Actuators B: Chem.*, vol. 373, 2022, Art. no. 132646.

[35] Z. Fan and J. G. Lu, "Gate-refreshable nanowire chemical sensors," *Appl. Phys. Lett.*, vol. 86, no. 12, 2005, Art. no. 123510.

[36] F. Mo, Y. Ardesi, M. R. Roch, M. Graziano, and G. Piccinini, "Investigation of amperometric sensing mechanism in gold–c60–gold molecular dot," *IEEE Sensors J.*, vol. 22, no. 20, pp. 19152–19161, Oct. 2022.

Open Access funding provided by 'Politecnico di Torino' within the CRUI CARE Agreement